A direct impedance tomography algorithm for locating small inhomogeneities

Martin Brühl[1]*, **Martin Hanke**[1], **Michael S. Vogelius**[2]**

[1] Fachbereich Mathematik, Johannes Gutenberg-Universität Mainz, 55099 Mainz, Germany; e-mail: bruehl@math.uni-mainz.de, hanke@math.uni-mainz.de
[2] Department of Mathematics, Rutgers University, New Brunswick, NJ 08903, USA; e-mail: vogelius@math.rutgers.edu

Date: May 28, 2001

Summary Impedance tomography seeks to recover the electrical conductivity distribution inside a body from measurements of current flows and voltages on its surface. In its most general form impedance tomography is quite ill-posed, but when additional a-priori information is admitted the situation changes dramatically. In this paper we consider the case where the goal is to find a number of small objects (inhomogeneities) inside an otherwise known conductor. Taking advantage of the smallness of the inhomogeneities, we can use asymptotic analysis to design a direct (i.e., noniterative) reconstruction algorithm for the determination of their locations. The viability of this direct approach is documented by numerical examples.

Mathematics Subject Classification (2000): 65N21, 35R30, 35C20

1 Introduction

Techniques for recovering the conductivity distribution inside a body from measurements of current flows and voltages on the body's surface go under the heading of electrical impedance tomography (EIT). The vast and growing literature reflects the many possible applications of this method, e.g. for medical diagnosis or nondestructive evaluation of materials. For further details we refer to the recent survey paper [8].

Since the underlying inverse problem is nonlinear and severely ill-posed it is generally advisable to incorporate all available a-priori knowledge

* Supported by the Deutsche Forschungsgemeinschaft (DFG) under grant HA 2121/2-3
** Supported by the National Science Foundation under grant DMS-0072556

about the unknown conductivity. One such type of knowledge could be that the body consists of a smooth background (of known conductivity) containing a number of unknown, small inclusions with a significantly higher or lower conductivity. This situation arises for example in mine detection, where one tries to locate the position of buried anti-personnel mines from electromagnetic data. The mines have a higher (metal) or lower (plastic) conductivity than the surrounding soil and they are small relative to the area being imaged. General purpose EIT reconstruction methods are likely to fail: due to the smallness of the mines the associated voltage potentials are very close to the potentials corresponding to the unperturbed medium, so unless one knows exactly what patterns to look for, noise will largely dominate the information contained in the measured data. Furthermore, in this application it is often not necessary to reconstruct the precise values of the conductivity of the mines or their shapes. The only information of real interest is their positions.

In this work we propose a direct algorithm for determining the positions of small conductivity inhomogeneities. The algorithm makes use of an asymptotic expansion of the voltage potentials, which has been derived by Cedio-Fengya et al. [6]; see also the prior work of Friedman and Vogelius [11] for the case of perfectly conducting or insulating inhomogeneities. Ammari et al. [1] have also utilized this asymptotic expansion to design a variationally based direct reconstruction method, a method that is quite different from the one presented here. Our algorithm is somewhat in the spirit of a method developed in [4,5], and it also has some similarities to a recent MUSIC-type method developed by Devaney [9]. A detailed discussion of the relation between the latter (MUSIC) algorithm and the linear sampling method in inverse scattering (cf. Kirsch [14]) is found in Cheney [7].

This paper is organized as follows. In the next section we review the asymptotic expansion of the voltage potentials in the presence of small inhomogeneities, in particular we show how this leads to a similar expansion for the associated Neumann-Dirichlet operator. The principal operator arising in the latter expansion will be examined in detail; this operator is at the root of our algorithm for the location of the inhomogeneities as explained in Section 3 and Section 4. In Section 5 we show how certain information about the shape of the inhomogeneities may be recovered, once their positions have been determined.

2 The forward problem with small inhomogeneities

Let $B \subset \mathbb{R}^n$, $n = 2, 3$, denote a bounded domain with a smooth boundary ∂B, and $\gamma(x)$ a smooth, positive background conductivity. We consider

conductivity distributions of the form

$$\gamma^\varepsilon(x) = \begin{cases} \kappa_j, & x \in \Omega_j^\varepsilon, \quad j = 1, \dots, p, \\ \gamma(x), & x \in B \setminus \bigcup_j \Omega_j^\varepsilon, \end{cases} \tag{2.1}$$

where $\Omega_j^\varepsilon = z_j + \varepsilon\Omega_j$. Here, the points z_j indicate the positions of the "centers" of the inhomogeneities, and the smooth sets Ω_j (with $0 \in \Omega_j$) describe their relative shapes. The "average" inhomogeneity size is specified by the parameter $\varepsilon > 0$, which is assumed to be small. We will also assume that $\gamma(z_j) \neq \kappa_j$, so that the constant conductivity of any inhomogeneity is different from that of the adjacent background.

If one induces a normal current flow f, with $\int_{\partial B} f\, ds = 0$, on the boundary ∂B, then this gives rise to a voltage potential u^ε that solves the Neumann boundary value problem

$$\nabla \cdot \gamma^\varepsilon \nabla u^\varepsilon = 0 \quad \text{in } B, \qquad \gamma^\varepsilon \frac{\partial u^\varepsilon}{\partial \nu} = f \quad \text{on } \partial B.$$

With the additional normalization condition $\int_{\partial B} u^\varepsilon\, ds = 0$ the solution u^ε becomes unique. The relation between the applied boundary currents f and the boundary voltages $u^\varepsilon|_{\partial B}$ defines a linear mapping $\Lambda^\varepsilon : f \mapsto u^\varepsilon|_{\partial B}$, the so-called Neumann-Dirichlet operator. Here we consider Λ^ε as an operator from $L^2_\diamond(\partial B)$ into itself, where $L^2_\diamond(\partial B) = \{f \in L^2(\partial B) : \int_{\partial B} f\, ds = 0\}$. In this topology Λ^ε is compact and selfadjoint.

We are interested in the behavior of Λ^ε as ε tends to zero, i.e., as the inhomogeneities Ω_j^ε shrink to the points z_j, $j = 1, \dots, p$. First of all, one expects that $u^\varepsilon|_{\partial B}$ converges to the boundary values of the potential u^0 corresponding to the background conductivity $\gamma^0 = \gamma$. This is indeed one conclusion of the following much more detailed result due to Cedio-Fengya et al. [6, Theorem 2].

Theorem 2.1 *Assume the points z_j, $j = 1, \dots, p$, satisfy*

$$\operatorname{dist}(z_i, z_j) \geq d_0 \quad \textit{for } i \neq j \qquad \textit{and} \qquad \operatorname{dist}(z_j, \partial B) \geq d_0 \tag{2.2}$$

for some constant $d_0 > 0$. Let $N(x, y)$ denote the Neumann function for the differential operator $\nabla \cdot \gamma \nabla$ in the domain B. Then, for $z \in \partial B$ one has the asymptotic expansion

$$u^\varepsilon(z) = u^0(z) + \varepsilon^n \sum_{j=1}^{p} \gamma(z_j) \frac{\gamma(z_j) - \kappa_j}{\kappa_j} \nabla_x N(z_j, z) \cdot M_j \nabla u^0(z_j) + \mathcal{O}(\varepsilon^{n+1/2}) \tag{2.3}$$

as $\varepsilon \to 0$. The symmetric positive definite $n \times n$-matrix M_j is the so-called polarization tensor corresponding to the j-th inhomogeneity.

The Neumann function $N(x,y)$ is the unique solution to

$$\nabla_x \cdot \gamma(x)\nabla_x N(x,y) = -\delta_y \quad \text{in } B, \quad \gamma(x)\frac{\partial N(x,y)}{\partial \nu_x} = -\frac{1}{|\partial B|} \quad \text{on } \partial B,$$

with the normalization $\int_{\partial B} N(x,y)\,ds_x = 0$. It is easy to see that N is symmetric, i.e., $N(x,y) = N(y,x)$ for $(x,y) \in B\times B\setminus \mathrm{diag}(B\times B)$. This symmetry yields a smooth extension of N to $(\overline{B}\times B \cup B\times\overline{B})\setminus \mathrm{diag}(B\times B)$ satisfying $\nabla_x N(z,\tilde{z}) = \nabla_y N(\tilde{z},z)$.

The polarization tensor M_j is a symmetric positive definite matrix, that depends on the relative shape of the j-th inhomogeneity Ω_j and the conductivity contrast $\gamma(z_j)/\kappa_j$. For its exact definition we refer to [6] (see also Appendix A of the present paper). In [11] and [6] it is assumed that the sets Ω_j are star-shaped, but as evidenced by [17] and [2] one may dispense with this condition in case the κ_j are strictly positive.

For the case of constant background conductivity there is a slight variation of Theorem 2.1, that for many practical applications is more useful, since it relies on an explicit fundamental solution. Let $\Phi(x,y)$ denote the function

$$\Phi(x,y) = \begin{cases} \frac{-1}{2\pi\gamma}\log|x-y|, & n=2, \\ \frac{1}{4\pi\gamma}|x-y|^{-1}, & n=3. \end{cases}$$

Theorem 2.2 *Assume the background conductivity γ is constant and that the points z_j, $j=1,\ldots,p$, satisfy condition* (2.2)*. Then, for $z \in \partial B$ one has the asymptotic expansion*

$$\begin{aligned} u^\varepsilon(z) - u^0(z) + 2\int_{\partial B}(u^\varepsilon(x)-u^0(x))\gamma\frac{\partial \Phi}{\partial \nu_x}(x,z)\,ds_x \\ = \; 2\varepsilon^n \sum_{j=1}^{p} \gamma\frac{\gamma-\kappa_j}{\kappa_j}\nabla_x\Phi(z_j,z)\cdot M_j \nabla u^0(z_j) + \mathcal{O}(\varepsilon^{n+1/2}) \end{aligned} \quad (2.4)$$

as $\varepsilon \to 0$ with M_j as in Theorem 2.1.

We note that for $f \in L^2_\diamond(\partial B)$ the functions u^ε and u^0 are not necessarily smooth up to the boundary ∂B. However, due to elliptic regularity results, the difference $u^\varepsilon(z) - u^0(z)$ is smooth (near) and up to the boundary ∂B. It is proved in [6] that the remainder terms in (2.3) and (2.4) are bounded by $C\varepsilon^{n+1/2}$, uniformly for $z \in \partial B$, however, numerical experiments suggest it is even smaller, namely of the order $\mathcal{O}(\varepsilon^{2n})$. The constant C in the bounds for the remainder terms depends on the domains Ω_j, B, the background conductivity γ, the constant d_0 and the normal current f. The dependence on f manifests itself through the need for an energy estimate and the need for pointwise bounds on the values and the derivatives of u^0 near the positions z_j — all of which only requires a bound on $\|f\|_{H^{-1/2}(\partial B)}$. In other

words, the dependence of C on f is only a dependence on $\|f\|_{H^{-1/2}(\partial B)}$. The details of this argument are found in [17] and [2] for the case of the Maxwell equations.

Let us now introduce the operator $D : L^2_\diamond(\partial B) \to L^2_\diamond(\partial B)$ defined by

$$Df = \sum_{j=1}^{p} \gamma(z_j) \frac{\gamma(z_j) - \kappa_j}{\kappa_j} \nabla_y N(\,\cdot\,, z_j) \cdot M_j \nabla u^0(z_j). \tag{2.5}$$

Since u^0 depends linearly on f this operator is linear, and from Theorem 2.1 (and the remark about the constant of the remainder term) it follows that

$$\Lambda^\varepsilon - \Lambda^0 = \varepsilon^n D + \mathcal{O}(\varepsilon^{n+1/2}), \tag{2.6}$$

where the remainder term $\mathcal{O}(\varepsilon^{n+1/2})$ is bounded by $C\varepsilon^{n+1/2}$ in the operator norm of $\mathcal{B}(H^{-1/2}_\diamond(\partial B), L^2_\diamond(\partial B))$ (and thus in the operator norm of $\mathcal{B}(L^2_\diamond(\partial B), L^2_\diamond(\partial B))$). Here we also used the fact that $\nabla_x N(z_j, z) = \nabla_y N(z, z_j)$ for $z \in \overline{B}$. The operator D is selfadjoint on $L^2_\diamond(\partial B)$, since it is the limit of the selfadjoint operators $\varepsilon^{-n}(\Lambda^\varepsilon - \Lambda^0)$.

In the rest of this section we will point out some additional properties of the operator D, which turn out to be crucial for our approach to determine the positions z_j. We begin by introducing another linear operator $G : L^2_\diamond(\partial B) \to \mathbb{R}^{n\times p}$

$$Gf = (\nabla u^0(z_1), \ldots, \nabla u^0(z_p)).$$

Here the potential u^0 corresponds to the input current f and can thus be represented as $u^0(y) = \int_{\partial B} N(x,y) f(x)\, ds_x$ for $y \in B$. Endowing $\mathbb{R}^{n\times p}$ with the standard Euclidean inner product,

$$\langle a, b\rangle_{\mathbb{R}^{n\times p}} = \sum_{j=1}^{p} a_j \cdot b_j$$
$$\text{for } a = (a_1, \ldots, a_p), b = (b_1, \ldots, b_p) \in \mathbb{R}^{n\times p}, a_j, b_j \in \mathbb{R}^n,$$

we then obtain

$$\begin{aligned}
\langle Gf, a\rangle_{\mathbb{R}^{n\times p}} &= \sum_{j=1}^{p} a_j \cdot \nabla u^0(z_j) \\
&= \sum_{j=1}^{p} a_j \cdot \int_{\partial B} \nabla_y N(x, z_j) f(x)\, ds_x \\
&= \Big\langle \sum_{j=1}^{p} a_j \cdot \nabla_y N(\,\cdot\,, z_j), f \Big\rangle_{L^2(\partial B)}
\end{aligned}$$

for arbitrary $a = (a_1, \ldots, a_p) \in \mathbb{R}^{n\times p}$. Therefore $G^* : \mathbb{R}^{n\times p} \to L^2_\diamond(\partial B)$ is given by

$$G^* a = \sum_{j=1}^{p} a_j \cdot \nabla_y N(\,\cdot\,, z_j). \tag{2.7}$$

Lemma 2.1 *G^* is injective.*

Proof Suppose that $G^*a = 0$ for $a = (a_1, \ldots, a_p) \in \mathbb{R}^{n\times p}$, or in other words,

$$\sum_{j=1}^{p} a_j \cdot \nabla_y N(x, z_j) = 0 \qquad \text{for } x \in \partial B.$$

Then the function $w(x) = \sum_{j=1}^{p} a_j \cdot \nabla_y N(x, z_j)$ solves the Cauchy problem

$$\nabla \cdot \gamma \nabla w = 0 \quad \text{in } B \setminus \bigcup_{j=1}^{p} \{z_j\}, \qquad w|_{\partial B} = 0, \qquad \gamma \frac{\partial w}{\partial \nu}\Big|_{\partial B} = 0,$$

and from the uniqueness of this problem (see for example [15, Theorem 19.II]) we deduce that $w \equiv 0$. If e_k denotes the k-th unit vector in $\mathbb{R}^n$, then in particular we have $\lim_{t\to 0} w(z_j + te_k) = 0$, and thus $e_k \cdot a_j = 0$. Indeed, otherwise the dipole singularity of $\nabla_y N(x, z_j)$ at z_j would imply $\lim_{t\to 0} |w(z_j + te_k)| = \infty$. This proves that $a_j = 0$, and thus the assertion of this lemma.

Corollary 2.1 *G is surjective.*

Proof This follows from Lemma 2.1 and the well-known relation $\mathcal{R}(G) = \mathcal{N}(G^*)^\perp$ between the ranges and null spaces of adjoint operators with finite rank.

Using the above formulae for G and G^* and the definition (2.5) of D, we see that these operators are related by

$$D = G^* M G, \tag{2.8}$$

where operator $M : \mathbb{R}^{n\times p} \to \mathbb{R}^{n\times p}$ is given by

$$Ma = \left(\gamma(z_1)\frac{\gamma(z_1) - \kappa_1}{\kappa_1} M_1 a_1, \ldots, \gamma(z_p)\frac{\gamma(z_p) - \kappa_p}{\kappa_p} M_p a_p\right)$$

for $a = (a_1, \ldots, a_p) \in \mathbb{R}^{n\times p}$. From the positive definiteness of the matrices M_j we conclude that D is positive (respectively negative) semidefinite, if $\kappa_j < \gamma(z_j)$ (respectively $\kappa_j > \gamma(z_j)$) for all $j = 1, \ldots, p$.

Let us take a closer look at the range of D. First we observe that $\mathcal{R}(D)$ is finite dimensional with dimension at most pn; more precisely we have

$$\mathcal{R}(D) \subset \operatorname{span}\big\{e_k \cdot \nabla_y N(\,\cdot\,, z_j)\big|_{\partial B} : \ k = 1, \dots, n; \ j = 1, \dots, p\big\}.$$

Next we show that this inclusion is actually an equality.

Proposition 2.1 *The range of D has dimension pn and is given by*

$$\mathcal{R}(D) = \operatorname{span}\big\{e_k \cdot \nabla_y N(\,\cdot\,, z_j)\big|_{\partial B} : \ k = 1, \dots, n; \ j = 1, \dots, p\big\}.$$

Proof The surjectivity of G and M implies $\mathcal{R}(D) = \mathcal{R}(G^* M G) = \mathcal{R}(G^*)$. This proposition is then an immediate consequence of the formula (2.7) for G^*.

Now we present the main tool for the identificaton of the positions z_j.

Proposition 2.2 *Let $d \in \mathbb{R}^n \setminus \{0\}$, $z \in B$, and $g_{z,d} = d \cdot \nabla_y N(\,\cdot\,, z)|_{\partial B}$. Then, $g_{z,d} \in \mathcal{R}(D)$ if and only if $z \in \{z_j : j = 1, \dots, p\}$.*

Proof Assume that $g_{z,d} \in \mathcal{R}(D)$. As a consequence of Proposition 2.1, $g_{z,d}$ may be represented as

$$g_{z,d}(x) = \sum_{j=1}^{p} a_j \cdot \nabla_y N(x, z_j) \qquad \text{for } x \in \partial B.$$

But then both $v(x) = \sum_{j=1}^{p} a_j \cdot \nabla_y N(x, z_j)$, and $d \cdot \nabla_y N(x, z)$ are solutions to the Cauchy problem

$$\nabla \cdot \gamma \nabla w = 0 \quad \text{in } B \setminus \big(\textstyle\bigcup_j \{z_j\} \cup \{z\}\big), \qquad w|_{\partial B} = g_{z,d}, \qquad \gamma \dfrac{\partial w}{\partial \nu}\Big|_{\partial B} = 0,$$

and from the uniqueness of solutions to this problem we conclude that $v(x) = d \cdot \nabla_y N(x, z)$ for $x \in B \setminus \big(\bigcup_j \{z_j\} \cup \{z\}\big)$. This is only possible if $z \in \{z_j : j = 1, \dots, p\}$, and so we have established the necessity of this condition. The sufficiency follows directly from Proposition 2.1.

Since the operator $\Lambda^\varepsilon - \Lambda^0$ is selfadjoint and compact on $L^2_\diamond(\partial B)$ it admits a spectral decomposition

$$\Lambda^\varepsilon - \Lambda^0 = \sum_{i=1}^{\infty} \lambda_i^\varepsilon v_i^\varepsilon (v_i^\varepsilon)^*, \qquad \|v_i^\varepsilon\|_{L^2(\partial B)} = 1,$$

with eigenvalues λ_i^ε decaying to zero. Similarly, the finite-dimensional self-adjoint operator D can be decomposed as

$$D = \sum_{i=1}^{pn} \lambda_i v_i v_i^*, \qquad \|v_i\|_{L^2(\partial B)} = 1,$$

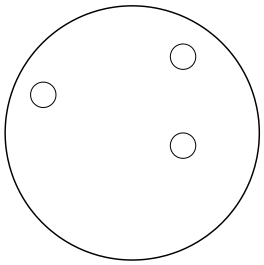

Fig. 2.1. Unit disk with three inhomogeneities.

(say with $|\lambda_1| \geq |\lambda_2| \geq \cdots \geq |\lambda_{pn}| > 0$). Using (2.6) and standard arguments from perturbation theory for linear operators [13], we get (by appropriate enumeration of the eigenvalues of $\Lambda^\varepsilon - \Lambda^0$) the following asymptotic formulae as $\varepsilon \to 0$,

$$\lambda_i^\varepsilon = \varepsilon^n \lambda_i + \mathcal{O}(\varepsilon^{n+1/2}), \qquad i = 1, 2, \ldots \tag{2.9}$$

Here we have set $\lambda_i = 0$ for $i > pn$. Let $P_m^\varepsilon : L^2_\diamond(\partial B) \to \text{span}\{v_1^\varepsilon, \ldots, v_m^\varepsilon\}$ and $P_m : L^2_\diamond(\partial B) \to \text{span}\{v_1, \ldots, v_m\}$ denote the orthogonal projectors

$$P_m^\varepsilon = \sum_{i=1}^m v_i^\varepsilon (v_i^\varepsilon)^* \qquad \text{and} \qquad P_m = \sum_{i=1}^m v_i v_i^*,$$

respectively. Suppose for simplicity the eigenvalues of D are simple; the limiting relationship (2.6) together with standard arguments from perturbation theory for linear operators [13] then gives

$$P_m^\varepsilon = P_m + \mathcal{O}(\varepsilon^{1/2}) \qquad \text{for } m \leq pn.$$

The same statement holds even if the eigenvalues are not simple, provided one makes "appropriate choices of eigenvectors" v_i^ε and v_i, $i = 1, 2, \ldots, np$.

We illustrate the asymptotic behaviour of the eigenvalues by means of a numerical example. In the unit disk $B \subset \mathbb{R}^2$ we choose $p = 3$ circular inhomogeneities, which are shown for $\varepsilon = 10^{-1}$ in Figure 2.1. The conductivity within each inhomogeneity is $\kappa = 0.5$ whereas $\gamma = 1$ is the the homogeneous background conductivity. The eigenvalues λ_i^ε of $\Lambda^\varepsilon - \Lambda^0$ for three different values of ε are shown in Figure 2.2. According to (2.9) we expect to see $pn = 6$ eigenvalues of order $\mathcal{O}(\varepsilon^2)$ while all the the remaining eigenvalues have smaller magnitude (no bigger than the remainder term in Theorem 2.1). In line with what we mentioned earlier this example suggests that the remainder term in Theorem 2.1 is indeed $\mathcal{O}(\varepsilon^{2n})$, and not just the $\mathcal{O}(\varepsilon^{n+1/2})$ asserted by our estimate.

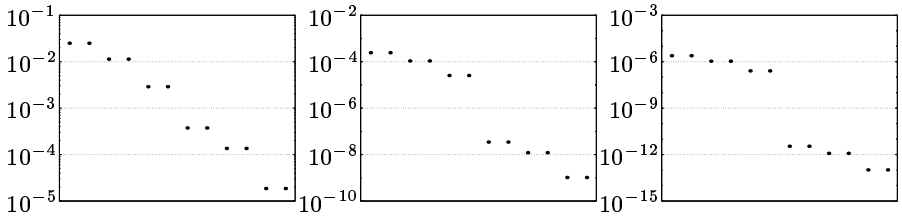

Fig. 2.2. Eigenvalues of $\Lambda^\varepsilon - \Lambda^0$ for $\varepsilon = 10^{-1}$, $\varepsilon = 10^{-2}$, and $\varepsilon = 10^{-3}$ (from left to right) for the example from Figure 2.1.

3 Determining the locations of the inhomogeneities based on the expansion from Theorem 2.1

Before we present our approach to determine the positions z_j we briefly recall the explicit characterization of the inclusions Ω_j^ε which has been derived in [4,5]. There it has been shown (provided $\Lambda^\varepsilon - \Lambda^0$ is semidefinite) that the parameter point z lies within one of the inclusions Ω_j^ε if and only if the series $\sum_{i=1}^\infty \langle v_i^\varepsilon, g_{z,d}\rangle^2_{L^2(\partial B)}/\lambda_i^\varepsilon$ converges. This is tested numerically by first estimating and then comparing the decay of the squared Fourier coefficients $\langle v_i^\varepsilon, g_{z,d}\rangle^2_{L^2(\partial B)}$ with the decay of the eigenvalues λ_i^ε. In order to apply such an algorithm, it is necessary to compute at least a few of these terms in a stable manner.

While the order of the Fourier coefficients is essentially independent of ε, the size of the largest eigenvalues decreases at least like $\mathcal{O}(\varepsilon^n)$ as ε tends to 0. Consequently, in the presence of data errors, the estimation of the decay rate of the eigenvalues will be impossible when the size ε of the unknown objects gets small.

The reconstruction method we propose here involves only the actual size of the Fourier coefficients $\langle v_i^\varepsilon, g_{z,d}\rangle_{L^2(\partial B)}$ (and to some extent the size of the eigenvalues) but not their decay rate. The present method is thus much less sensitive to noise. The eigenvalues are only used to identify the subspace corresponding to the pn largest eigenvalues. This is possible if these eigenvalues exceed the noise level.

In Proposition 2.2 we have seen that a test point z coincides with one of the positions z_j if and only if $g_{z,d} = d \cdot \nabla_y N(\cdot, z)|_{\partial B} \in \mathcal{R}(D)$, or equivalently, if $(I - P_{pn})g_{z,d} = 0$. In other words, if we decompose the test function orthogonally as $g_{z,d} = P_{pn}g_{z,d} + (I - P_{pn})g_{z,d}$ and define the angle $\theta(z) \in [0, \pi/2]$ by

$$\cot\theta(z) = \frac{\|P_{pn}g_{z,d}\|}{\|(I - P_{pn})g_{z,d}\|},$$

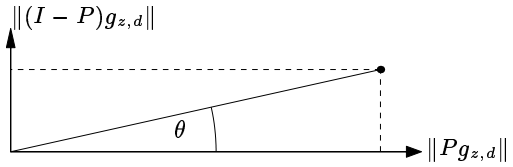

Fig. 3.1. Definition of the angle θ.

cf. Figure 3.1, then we have that

$$z \in \{z_j : j = 1, \ldots, p\} \quad \Longleftrightarrow \quad \theta(z) = 0 \quad \Longleftrightarrow \quad \cot\theta(z) = \infty.$$

Unfortunately, we cannot compute $\theta(z)$, because P_{pn} depends on the unknown positions z_j. However, for small sizes ε the projected test function $P_{np}g_{z,d}$ is well approximated by $P^\varepsilon_{pn}g_{z,d}$, and the projections P^ε_m can be computed for each m by means of the eigenfunctions of the measured operator $\Lambda^\varepsilon - \Lambda^0$.

This may serve as a motivation for the following definition of the angle $\theta^\varepsilon_m(z)$ by

$$\cot\theta^\varepsilon_m(z) = \frac{\|P^\varepsilon_m g_{z,d}\|}{\|(I-P^\varepsilon_m)g_{z,d}\|} = \left(\frac{\sum\limits_{i\le m} \langle v^\varepsilon_i, g_{z,d}\rangle^2_{L^2(\partial B)}}{\sum\limits_{i>m} \langle v^\varepsilon_i, g_{z,d}\rangle^2_{L^2(\partial B)}} \right)^{1/2}.$$

For $z \in \{z_j : j = 1, \ldots, p\}$ all terms in the denominator are of order $o(1)$ as $\varepsilon \to 0$ if m is chosen equal to pn. The numerical value of pn may be estimated by looking for a "gap" in the set of eigenvalues of $\Lambda^\varepsilon - \Lambda^0$. If we plot $\cot\theta^\varepsilon_{pn}(z)$ as a function of z, we thus expect to see large values for points z which are close to the actual positions z_j. Since none of the eigenvectors of $\Lambda^\varepsilon - \Lambda^0$ corresponding to eigenvalues λ^ε_i, $i > np$, are exactly of the form $g_{z,d}$, $z \notin \{z_j : j = 1, \ldots, p\}$, we expect the same to be true if we plot $\cot\theta^\varepsilon_m(z)$ for moderate size $m > pn$.

The calculation of $\cot\theta^\varepsilon_m(z)$ requires the calculation of $g_{z,d} = d \cdot \nabla_y N(\,\cdot\,, z)|_{\partial B}$, something that in most cases will be quite expensive. One notable exception occurs when $n = 2$, the background medium has constant conductivity, and B is a disk (for example $B = \{x : |x| < 1\}$). In this case the Neumann function has an explicit expression, that we may use to calculate the boundary values of its gradient. This calculation yields the simple formula

$$\nabla_y N(x,z) = \frac{1}{\gamma\pi}\frac{x-z}{|x-z|^2} \qquad \text{for } x \in \partial B,\ z \in B.$$

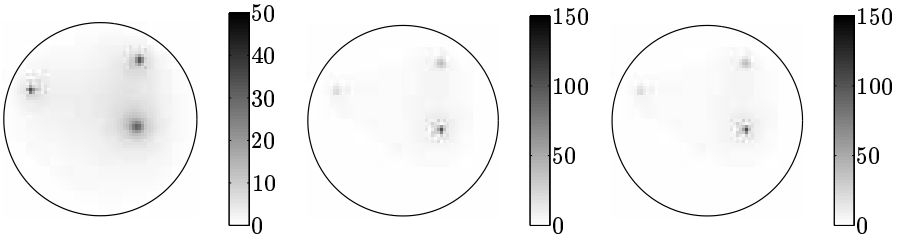

Fig. 3.2. Example with three inclusions: $\cot\theta_6^\varepsilon(z)$ for $\varepsilon = 10^{-1}$, $\varepsilon = 10^{-2}$, and $\varepsilon = 10^{-3}$.

When the background medium has constant conductivity, but the domain B is not a disk, one may utilize the formula

$$g_{z,d} = d \cdot \nabla_y N(\,\cdot\,, z)|_{\partial B} = Q(\Psi_{z,d}|_{\partial B}) - \Lambda^0\Big(\frac{\partial \Psi_{z,d}}{\partial \nu}|_{\partial B}\Big)$$

with

$$\Psi_{z,d}(x) = d \cdot \nabla_y \Phi(x, z), \qquad x \in \overline{B} \setminus \{z\},$$

and Q denoting the projection operator from $L^2(\partial B)$ onto $L^2_\diamond(\partial B)$,

$$Qf = f - \frac{1}{|\partial B|}\int_{\partial B} f(x)\, ds_x. \tag{3.1}$$

The presence of the operator Λ^0 renders the computation of $g_{z,d}$ somewhat expensive, and since this computation typically has to be carried out for a very large number of test points z, one may, for non-circular B, prefer to use the approach we describe in Section 4.

For the two-dimensional example from Figure 2.1, using synthetic data without noise, we show plots of $\cot\theta_6^\varepsilon(z)$ in Figure 3.2 for three values of ε. The centers of the three circular inhomogeneities are clearly determined in each case. Note that a-priori knowledge of ε is not required for the computation of $\theta_m^\varepsilon(z)$; only the spectral decomposition of the measured operator $\Lambda^\varepsilon - \Lambda^0$ is involved.

In Figure 3.3 we consider an example with $p = 7$ circular inhomogeneities with radius $\varepsilon = 10^{-2}$ (still inside the two-dimensional unit disk) and we plot $\cot\theta_m^\varepsilon(z)$ for different values of m.

Indeed, for $m \geq pn = 14$ the seven centers are well reconstructed, whereas for smaller m the plots give misleading results. This easily computable sequence of plots yields remarkably good information on both the number of inhomogeneities as well as on their location. When comparing the method proposed here to other methods that have been designed for imaging small inhomogeneities, it is fair to point out that it uses information about the entire Neumann-Dirichlet map. In contrast, the iterative approach taken in [6] only relies on a single set of Cauchy data (a single

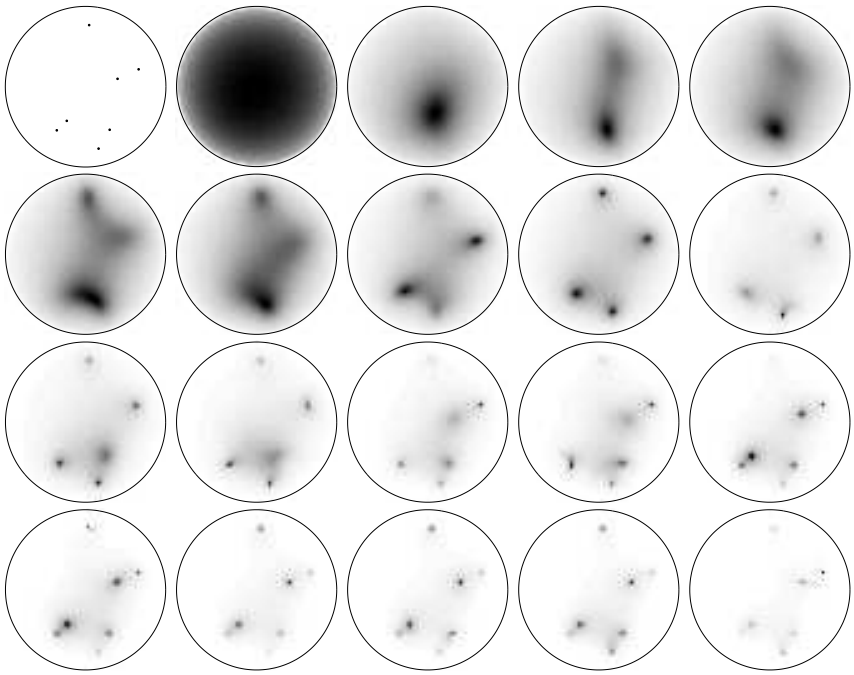

Fig. 3.3. Actual positions (upper left picture) of seven inclusions and $\cot \theta_m^\varepsilon(z)$ for $m = 1, \ldots, 19$.

point on the graph of the Neumann-Dirichlet map) and not surprisingly, it is more limited in its ability to effectively locate a high number of inhomogeneities. At this point it also seems relevant to point out that the use of spectral data from the (Neumann-Dirichlet) boundary map is not new in impedance imaging. It was for instance very early noticed, that the use of imposed boundary currents closely approximating eigenvectors is very advantageous [12].

4 Determining the locations of the inhomogeneities based on the expansion from Theorem 2.2

As mentioned in the last section the required calculation of the gradient of the Neumann function is often quite costly. If the background medium is truly inhomogeneous (non-constant) then there is not much that can be done about this. However, if the background medium has constant conductivity, then it is possible to slightly change the algorithm we have developed so far, such as to lower this cost significantly. For that purpose we rely on the

asymptotic formula of Theorem 2.2. This formula asserts that

$$(I+K)(\Lambda^\varepsilon - \Lambda^0) = \varepsilon^n E + \mathcal{O}(\varepsilon^{n+1/2}), \tag{4.1}$$

where E is the finite rank operator $L^2_\diamond(\partial B) \to L^2(\partial B)$ defined by

$$Ef = \sum_{j=1}^{p} 2\gamma \frac{\gamma-\kappa_j}{\kappa_j} \nabla_y \Phi(\,\cdot\,, z_j) \cdot M_j \nabla u^0(z_j), \tag{4.2}$$

and K is the compact operator $L^2(\partial B) \to L^2(\partial B)$ defined by

$$Kf = 2\gamma \int_{\partial B} \frac{\partial \Phi}{\partial \nu_x}(x,\,\cdot\,) f(x)\, ds_x.$$

The remainder is bounded by $C\varepsilon^{n+1/2}$ in the operator norm on $\mathcal{B}(L^2_\diamond(\partial B); L^2(\partial B))$. The adjoint $K^* : L^2(\partial B) \to L^2(\partial B)$ of the operator K has the representation

$$K^* f = 2\gamma \int_{\partial B} \frac{\partial \Phi}{\partial \nu_y}(x,\,\cdot\,) f(x)\, ds_x.$$

A simple calculation shows that $\int_{\partial B} K^* f(y)\, ds_y = -\int_{\partial B} f(x)\, ds_x$, from which it follows that K^* maps $L^2_\diamond(\partial B)$ into itself. Furthermore, $I+K^*$ is one-to-one and onto as an operator $L^2_\diamond(\partial B) \to L^2_\diamond(\partial B)$ — this follows from its direct relationship to the solution of the interior Neumann problem (see for example [10, Proposition 3.37]). By appropriate multiplication of (4.1) by $I+K^*$ and by the projector Q from (3.1) we obtain

$$Q(I+K)(\Lambda^\varepsilon - \Lambda^0)(I+K^*)Q = \varepsilon^n QE(I+K^*)Q + \mathcal{O}(\varepsilon^{n+1/2}). \tag{4.3}$$

The operators $Q(I+K)(\Lambda^\varepsilon - \Lambda^0)(I+K^*)Q$ and $QE(I+K^*)Q$ are selfadjoint on $L^2(\partial B)$, and just as in the previous section we may now use the measured data $(\Lambda^\varepsilon - \Lambda^0)$ to approximately calculate the range of $QE(I+K^*)Q$. If B is a disk (in two dimensions) then $I+K = I+K^* = I$ on $L^2_\diamond(\partial B)$ and $QE = D$, and the formula (4.3) is thus identical with (2.6). In the general case we have a result similar to Proposition 2.1.

Proposition 4.1 *The range of $QE(I+K^*)Q$ is given by*

$$\begin{aligned}\mathcal{R}(QE(I+K^*)Q) &= \mathcal{R}(QE)\\ &= \operatorname{span}\big\{ Q\big(e_k \cdot \nabla_y \Phi(\,\cdot\,, z_j)\big|_{\partial B}\big) :\ k=1,\dots,n;\ j=1,\dots,p\big\}.\end{aligned}$$

Proof The fact that $(I+K^*)Q$ maps $L^2(\partial B)$ onto $L^2_\diamond(\partial B)$ yields that $\mathcal{R}(QE(I+K^*)Q) = \mathcal{R}(QE)$. As in Section 2, the operator

$$MG : f \to \Big(\gamma \frac{\gamma-\kappa_1}{\kappa_1} M_1 \nabla u^0(z_1), \dots, \gamma \frac{\gamma-\kappa_p}{\kappa_p} M_p \nabla u^0(z_p)\Big)$$

maps $L^2_\diamond(\partial B)$ onto $\mathbb{R}^{n\times p}$. It is now obvious from the definition of E, cf. (4.2), that

$$\mathcal{R}(E) = \operatorname{span}\big\{ e_k \cdot \nabla_y \Phi(\,\cdot\,, z_j)\big|_{\partial B} :\ k = 1,\dots,n;\ j = 1,\dots,p \big\},$$

from which the assertion follows.

To obtain an equivalent of Proposition 2.2 we must insist that

Assumption I

For any set of $p+1$ distinct points $\{z_j\}_{j=1}^{p+1}$ in B, the $(p+1)n$ functions $\{Q\big(e_k \cdot \nabla_y \Phi(\,\cdot\,, z_j)\big|_{\partial B}\big)\}_{k=1,j=1}^{n,p+1}$ are linearly independent.

Proposition 4.2 *Suppose Assumption I is satisfied. Let $d \in \mathbb{R}^n \setminus \{0\}$, $z \in B$, and let $h_{z,d} \in L^2_\diamond(\partial B)$ denote the function $h_{z,d} = Q\big(d\cdot\nabla_y\Phi(\,\cdot\,,z)|_{\partial B}\big)$. Then $h_{z,d} \in \mathcal{R}(QE)$ if and only if $z \in \{z_j : j = 1,\dots,p\}$.*

Proof This is an immediate consequence of the linear independency assumption (Assumption I) applied to the $p+1$ points $\{z\} \cup \{z_j\}_{j=1}^p$, and the characterization of $\mathcal{R}(QE)$ obtained in Proposition 4.1.

As we have seen earlier a two-dimensional disk satisfies the Assumption I (this is verified in the proof of Proposition 2.2) but there are many other such domains, as witnessed by the following result.

Proposition 4.3 *Assumption I is satisfied for any bounded, convex, two-dimensional domain B, the boundary of which contains a straight line segment.*

Proof Pick a coordinate system (s,t) such that the boundary of B shares a line segment with the s-axis and such that B lies in the half-plane $t > 0$. Let (s_j, t_j) denote the coordinates of the points z_j, $j = 1,\dots,p+1$. In the (s,t) coordinate system the function $a_j \cdot \nabla_y \Phi(\,\cdot\,, z_j) = \frac{1}{2\pi\gamma}\frac{a_j\cdot(x-z_j)}{|x-z_j|^2}$ has the expression

$$a_j \cdot \nabla_y \Phi(\,\cdot\,, z_j) = \frac{1}{2\pi\gamma}\frac{a_j^{(1)}(s-s_j) + a_j^{(2)}(t-t_j)}{(s-s_j)^2 + (t-t_j)^2},$$

where $(a_j^{(1)}, a_j^{(2)}) \in \mathbb{R}^2$ are the (s,t) coordinates of the vector a_j. Therefore

$$Q\big(a_j \cdot \nabla_y \Phi(\,\cdot\,, z_j)\big|_{\partial B}\big) = \frac{1}{2\pi\gamma}\frac{a_j^{(1)}(s-s_j) - a_j^{(2)} t_j}{(s-s_j)^2 + t_j^2} + c_j$$

on the common line segment (say $0 < s < S$) that ∂B shares with the s-axis. In order to verify this lemma we have to show that

$$\sum_{j=1}^{p+1} Q\big(a_j \cdot \nabla_y \Phi(\,\cdot\,, z_j)\big|_{\partial B}\big) = 0$$

for some set of vectors $a_j \in \mathbb{R}^2$, implies that $a_j = 0$ for all $j = 1, \ldots, p+1$. We do this by showing that

$$\sum_{j=1}^{p+1} \left(\frac{a_j^{(1)}(s - s_j) - a_j^{(2)} t_j}{(s - s_j)^2 + t_j^2} + c_j \right) = 0, \qquad 0 < s < S, \tag{4.4}$$

implies $a_j^{(1)} = a_j^{(2)} = 0$ for all $j = 1, \ldots, p+1$. The expression that appears on the left hand side of (4.4) is a meromorphic function (of $s \in \mathbb{C}$) and if either $a_j^{(1)} \in \mathbb{R}$ or $a_j^{(2)} \in \mathbb{R}$ is not zero then it has proper poles at $s = s_j \pm i t_j$. Here we use that $\{s_j \pm i t_j\}_{j=1}^{p+1}$ are $2(p+1)$ distinct complex numbers, as follows from the fact that the points $\{z_j\}_{j=1}^{p+1} = \{(s_j, t_j)\}_{j=1}^{p+1}$ are distinct and the fact that each t_j is positive. The presence of these proper poles, however, would contradict the fact that the left hand side of (4.4) identically vanishes on the real interval $0 < s < S$. We conclude that $a_j^{(1)} = a_j^{(2)} = 0$, $j = 1, \ldots, p+1$, as desired.

The modified reconstruction algorithm proceeds just as in Section 3, using the spectral decomposition of the operator $Q(I + K)(\Lambda^\varepsilon - \Lambda^0)(I + K^*)Q$ in place of that of $\Lambda^\varepsilon - \Lambda^0$, and using the explicit functions $h_{z,d}$ in place of $g_{z,d}$.

5 Recovering other geometric information

In this section we presume for the moment that the positions, z_j, of the inhomogeneities have already been reconstructed, and that we now seek to recover information about their shape.

First, let us make the simplifying assumption that B is the unit disk in $\mathbb{R}^2$, and that the background conductivity γ is constant. In this case the approach based on the expansion from Theorem 2.1 is quite simple, since the function $\nabla_y N(\,\cdot\,, z)\big|_{\partial B}$ is known explicitly; as mentioned earlier it is given by

$$\nabla_y N(x, z) = \frac{1}{\gamma\pi} \frac{x - z}{|x - z|^2} \qquad \text{for } x \in \partial B,\ z \in B.$$

We shall consider the two input currents $f_l = \nu_l = e_l \cdot \nu$, $l = 1, 2$, for which $u_l^0(x) = \frac{1}{\gamma} x_l$ are the resulting harmonic potentials, and so $\nabla u_l^0(x) = \frac{1}{\gamma} e_l$.

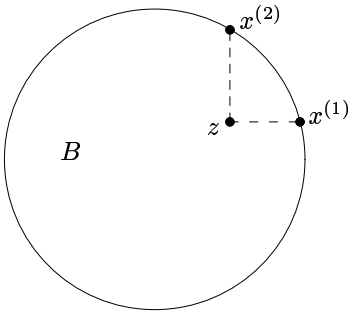

Fig. 5.1. Selection of the points $x^{(1)}$ and $x^{(2)}$.

We assume for simplicity that only one inhomogeneity is present in B having center z, and polarization tensor M. We choose the two points $x^{(1)}$ and $x^{(2)}$ on the boundary ∂B so that $x^{(k)} - z = |x^{(k)} - z| e_k$, $k = 1, 2$, cf. Figure 5.1. Then we have

$$Df_l(x^{(k)}) = \gamma \frac{\gamma - \kappa}{\kappa} \frac{e_k}{\gamma\pi |x^{(k)} - z|} \cdot M \frac{e_l}{\gamma} = \frac{\gamma - \kappa}{\kappa\gamma\pi |x^{(k)} - z|} m_{kl}. \quad (5.1)$$

From our data we have available the voltage differences

$$(\Lambda^\varepsilon - \Lambda^0) f_l(x^{(k)}) \approx \varepsilon^2 Df_l(x^{(k)}), \qquad k, l = 1, 2,$$

and we may thus approximately recover the scaled polarization tensor

$$\tilde{M} = \varepsilon^2 \frac{\gamma - \kappa}{\gamma\kappa} M.$$

We now discuss the kind of information about the unknown object that can be gained from this data.

Suppose the inhomogeneity has the form $z + \varepsilon\mathcal{E}$ where $\mathcal{E}$ is the ellipse given by $\mathcal{E} = \{x : x^* A x \le 1\}$ (here A is a symmetric positive definite 2×2-matrix). Let $R = \left(\begin{smallmatrix} c & -s \\ s & c \end{smallmatrix}\right)$ with $c = \cos\varphi$, $s = \sin\varphi$, $0 \le \varphi < \pi$, be the rotation matrix, for which the focal interval of the rotated ellipse $\mathcal{E}' = R^* \mathcal{E}$ lies on the x_1-axis, i.e., for which

$$\mathcal{E}' = \{x : x^* A' x \le 1\} \qquad \text{with} \qquad A' = R^* A R = \begin{pmatrix} 1/a^2 & 0 \\ 0 & 1/b^2 \end{pmatrix}.$$

Here a, b, $a \ge b$, denote the lengths of the two semi axes of the ellipse. In Appendix A we sketch how the associated polarization tensor M' of $\mathcal{E}'$ may be calculated explicitly. The resulting formula is

$$\tilde{M}' = \varepsilon^2 \frac{\gamma - \kappa}{\gamma\kappa} M' = \frac{\varepsilon^2 |\mathcal{E}|}{\gamma} (\mu - 1)(1 + q) \begin{pmatrix} \frac{1}{\mu + q} & 0 \\ 0 & \frac{1}{1 + \mu q} \end{pmatrix} = \begin{pmatrix} \lambda_1 & 0 \\ 0 & \lambda_2 \end{pmatrix}$$

with

$$\lambda_1 = \frac{|\varepsilon\mathcal{E}|}{\gamma}\frac{(\mu-1)(1+q)}{\mu+q} \qquad \text{and} \qquad \lambda_2 = \frac{|\varepsilon\mathcal{E}|}{\gamma}\frac{(\mu-1)(1+q)}{1+\mu q}. \quad (5.2)$$

Here $q = b/a \in (0,1]$ and $\mu = \gamma/\kappa \in [0,\infty] \setminus \{1\}$ denote the aspect ratio of the semi axes of the ellipse and the contrast of the conductivities, respectively. Note that $\lambda_1 \leq \lambda_2$ for all admissible values of q and μ. The scaled polarization tensor of the original ellipse $\mathcal{E}$ is then given by $\tilde{M} = R\tilde{M}'R^*$.

We note that the matrix A describing the geometry of the ellipse and the scaled polarization tensor $\tilde{M}$ are diagonalized by the same rotation matrix R; to be more precise, the common set of eigenvectors is specified by the semi axes of the ellipse $\mathcal{E}$. Consequently, the orientation of the ellipse can be recovered from knowledge of the eigenvectors of $\tilde{M}$.

The four remaining unknown quantities are the conductivities γ, κ, and the lengths εa and εb of the semi axes of the ellipse. An equivalent set of parameters are γ, μ, q, and $|\varepsilon\mathcal{E}|$.

The background conductivity γ is in practice either a-priori known, or can easily be estimated from the homogeneous potential data for the induced input current $f = \nu_l$. Indeed, in this case $u^0(x) = \frac{1}{\gamma}x_l$ is the associated voltage measurement, from which one can estimate γ.

This means that actually three quantities remain to be identified, namely q, μ, and the area $|\varepsilon\mathcal{E}|$ of the unknown ellipse. However, the eigenvalues of $\tilde{M}$ give only two pieces of data. Therefore, we need further information about the inhomogeneities, in the form of a-priori knowledge about their shape, size, or conductivity. For example, if μ is known, then from (5.2) we can compute q and $|\varepsilon\mathcal{E}|$ by

$$q = \frac{\lambda_2 - \mu\lambda_1}{\lambda_1 - \mu\lambda_2} \qquad \text{and} \qquad |\varepsilon\mathcal{E}| = \gamma\frac{\mu+1}{\mu-1}\left(\frac{1}{\lambda_1}+\frac{1}{\lambda_2}\right)^{-1}. \quad (5.3)$$

In many practically relevant situations the conductivity contrast will be rather high, i.e., we will have $\mu \gg 1$ or $\mu \ll 1$. As a simplification we might assume that $\mu = \infty$, if $\tilde{M}$ is positive definite, and we might assume that $\mu = 0$, if $\tilde{M}$ is negative definite. Using these extreme values in (5.3) we obtain

$$q = \min\left(\frac{\lambda_1}{\lambda_2}, \frac{\lambda_2}{\lambda_1}\right) \qquad \text{and} \qquad |\varepsilon\mathcal{E}| = \gamma\left|\frac{1}{\lambda_1}+\frac{1}{\lambda_2}\right|^{-1}. \quad (5.4)$$

The lengths of the semi axes of the ellipse can then be expressed as follows,

$$\varepsilon a = \sqrt{\frac{|\varepsilon\mathcal{E}|}{\pi q}} \qquad \text{and} \qquad \varepsilon b = \sqrt{\frac{|\varepsilon\mathcal{E}|q}{\pi}}. \quad (5.5)$$

		phantom data	reconstructed data
background conductivity	γ	1	1.0005
position	z	$(0.333,\ 0.667)$	$(0.334,\ 0.667)$
scaled polarization tensor	$10^4 \cdot \tilde{M}$	$\begin{pmatrix} 14.73 & -6.56 \\ -6.56 & 22.31 \end{pmatrix}$	$\begin{pmatrix} 14.76 & -6.61 \\ -6.60 & 22.33 \end{pmatrix}$
eigenvalues	$10^4 \cdot (\lambda_1,\ \lambda_2)$	$(10.94,\ 26.10)$	$(10.94,\ 26.16)$
rotation angle	φ	30°	30.10°
lengths of semi axes	$10^2 \cdot (\varepsilon a,\ \varepsilon b)$	$(3,\ 1)$	$(2.42,\ 1.01)$
conductivity in ellipse	κ	0.1	0 (assumption)

Table 5.1. Reconstruction of an ellipse.

We illustrate the reconstruction procedure by a numerical example. As a phantom we choose a small ellipse within the unit disk, with a much lower conductivity than that of the background. The geometry of this ellipse is specified in Table 5.1. Synthetic measurements are generated using a standard boundary element method.

In the first step we locate the position of the inhomogeneity by employing the technique introduced in Section 3. The position z is found as the point, where $\cot \theta_2^\varepsilon(z)$ attains its maximum. Afterwards the scaled polarization tensor $\tilde{M}$ is recovered from (5.1). A spectral decomposition of $\tilde{M}$ yields the orientation of the ellipse. Finally, the lengths of the semi axes are obtained from (5.4) and (5.5).

In two further numerical experiments we choose phantoms of different shape. The same algorithm as before yields an ellipse with a scaled polarization tensor as given by the data (that ellipses are sufficient to fit the data is a well known fact, see [16]). If the original shape is close to an ellipse then we can hope that this reconstruction provides a good approximation. This is illustrated in Figure 5.2, where we have chosen phantoms in the shape of a kidney (left) and a boomerang (right); the conductivity contrast for the calculation of the synthetic data was taken to be $\mu = 100$ in both cases. The original phantom is drawn with a thick solid line, and a thin solid line is used for the reconstructed ellipse in the absence of noise. The adjacent boxes zoom in on the region of interest. We also performed experiments with noisy data, where the measurements were perturbed by adding 0.5% relative noise. The corresponding reconstructions are shown in dashed lines.

A Polarization tensor for an ellipse

According to [6] the entries of the polarization tensor $M = (m_{kl})$ corresponding to a small inclusion "centered" at z_0, of relative shape Ω, and

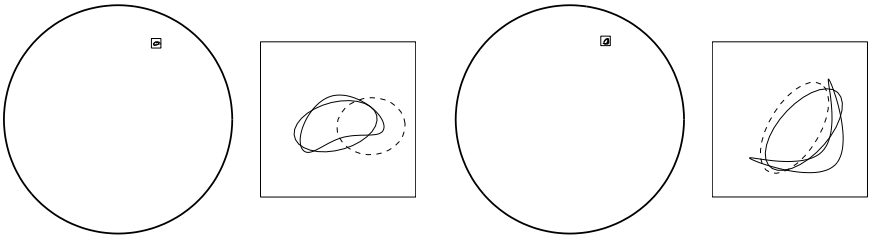

Fig. 5.2. Reconstruction of non-elliptic objects without noise (solid ellipse) and with 0.5% noise (dashed ellipse).

with conductivity κ are given by

$$m_{kl} = |\Omega|\delta_{kl} - \int_{\partial\Omega} y_k \frac{\partial \phi_l^+}{\partial \nu}\, ds_y, \qquad k,l = 1,\dots,n.$$

Here, the functions $\phi_l(y)$ are the solutions to the following problem:

$$\Delta\phi_l = 0 \quad \text{in } \Omega \text{ and in } \mathbb{R}^n \setminus \overline{\Omega}, \tag{A.1a}$$

$$\phi_l^+ = \phi_l^- \quad \text{on } \partial\Omega, \tag{A.1b}$$

$$\gamma(z_0)\frac{\partial \phi_l^+}{\partial \nu} - \kappa\frac{\partial \phi_l^-}{\partial \nu} = (\gamma(z_0) - \kappa)\nu_l \quad \text{on } \partial\Omega, \tag{A.1c}$$

$$\lim_{|y|\to\infty} \phi_l(y) = 0, \tag{A.1d}$$

where the $+$ and $-$ superscripts denote the limits on $\partial\Omega$ from the exterior and interior of Ω, respectively. It is not difficult to calculate that if Ω is a two-dimensional disk, then the associated polarization tensor is a multiple of the identity matrix, namely

$$M = |\Omega| \begin{pmatrix} \frac{2\kappa}{\gamma+\kappa} & 0 \\ 0 & \frac{2\kappa}{\gamma+\kappa} \end{pmatrix}. \tag{A.2}$$

Here we will calculate M in the case Ω equals $\mathcal{E}'$, an ellipse with focal interval $[-c, c]$ on the x_1-axis and eccentricity $1/\cosh\rho$, or in other words, an ellipse whose semi-major axis is of length $a = c\cosh\rho$ and lies on the x_1-axis, and whose semi-minor axis is of length $b = c\sinh\rho$ and lies on the x_2-axis.

First we have to solve the boundary value problems (A.1) in order to determine the functions ϕ_1 and ϕ_2. In order to do this, we introduce elliptic coordinates (r, ω),

$$x_1 = c\cos\omega\cosh r, \qquad x_2 = c\sin\omega\sinh r, \qquad (r \geq 0,\ 0 \leq \omega < 2\pi),$$

in which the ellipse is given by $\mathcal{E}' = \{(r,\omega) : r < \rho\}$. Separation of variables yields a general solution of the Laplace equation of the form

$$\phi(r,\omega) = A_0 + \sum_{m=1}^{\infty} (A_m \cos m\omega\, e^{-mr} + B_m \sin m\omega\, e^{-mr} + C_m \cos m\omega\, e^{mr} + D_m \sin m\omega\, e^{mr})$$

in $\mathcal{E}' \setminus [-c,c]$ and in the exterior of $\mathcal{E}'$ (with different sets of coefficients). For the solution in $\mathcal{E}' \setminus [-c,c]$ to extend to a harmonic function in $\mathcal{E}'$ we must furthermore require that

$$\phi(0,\omega) = \phi(0,-\omega) \quad \text{and} \quad \frac{\partial\phi}{\partial r}(0,\omega) = -\frac{\partial\phi}{\partial r}(0,-\omega), \qquad \omega \in [0,2\pi). \tag{A.3}$$

The coefficients of the specific solutions ϕ_1 and ϕ_2 are now determined by the conditions (A.3) and the boundary conditions (A.1b)–(A.1d). The result is

$$\phi_1(r,\omega) = \tfrac{(\kappa-\gamma)ab}{\gamma a+\kappa b} R_1(r)\cos\omega \quad \text{and} \quad \phi_2(r,\omega) = \tfrac{(\kappa-\gamma)ab}{\gamma b+\kappa a} R_2(r)\sin\omega$$

with

$$R_1(r) = \begin{cases} \frac{\cosh r}{\cosh\rho} & \text{for } r<\rho, \\ \frac{e^{-r}}{e^{-\rho}} & \text{for } r>\rho, \end{cases} \quad \text{and} \quad R_2(r) = \begin{cases} \frac{\sinh r}{\sinh\rho} & \text{for } r<\rho, \\ \frac{e^{-r}}{e^{-\rho}} & \text{for } r>\rho. \end{cases}$$

Using this it turns out that the polarization tensor M' takes diagonal form, namely

$$M' = |\mathcal{E}'| \begin{pmatrix} \frac{\kappa(a+b)}{\gamma a+\kappa b} & 0 \\ 0 & \frac{\kappa(a+b)}{\gamma b+\kappa a} \end{pmatrix}, \tag{A.4}$$

where $|\mathcal{E}'| = \pi ab$ is the area of the ellipse. Note that for the special case of a disk we have $a = b$ and then (A.4) reduces to (A.2).

For an arbitrary ellipse $\mathcal{E}$ whose semi axes are not aligned with the coordinate axes, one can find an orthogonal transformation R such that $\mathcal{E} = R\mathcal{E}'$, where $\mathcal{E}'$ is of the above form. The polarization tensor M corresponding to $\mathcal{E}$ is then given by $M = RM'R^*$, cf. [11, Section 6].

References

1. Ammari, H., Moskow, S., Vogelius, M. S.: Boundary integral formulae for the reconstruction of electric and electromagnetic inhomogeneities of small volume. Submitted.
2. Ammari, H., Vogelius, M. S., Volkov, D.: Asymptotic formulas for perturbations in the electromagnetic fi elds due to the presence of inhomogeneities of small diameter II. The full Maxwell equations. To appear in J. Math. Pures Appl., IX. Sér.

3. Borcea, L., Berryman, J. G., Papanicolaou, G. C. (1996): High-contrast impedance imaging. Inverse Probl. **12**, 835–858.
4. Brühl, M. (2001): Explicit characterization of inclusions in electrical impedance tomography. SIAM J. Math. Anal. **32**, 1327–1341.
5. Brühl, M., Hanke, M. (2000): Numerical implementation of two noniterative methods for locating inclusions by impedance tomography. Inverse Probl. **16**, 1029–1042.
6. Cedio-Fengya, D. J., Moskow, S., Vogelius, M. S. (1998): Identification of conductivity imperfections of small diameter by boundary measurements. Continuous dependence and computational reconstruction. Inverse Probl. **14**, 553–595.
7. Cheney, M.: The linear sampling method and the MUSIC algorithm. To appear in Inverse Probl.
8. Cheney, M., Isaacson, D., Newell, J. C. (1999): Electrical impedance tomography. SIAM Rev. **41**, 85–101.
9. Devaney, A. J.: Super-resolution processing of multi-static data using time reversal and MUSIC. To appear in J. Acoust. Soc. Am.
10. Folland, G. B. (1976): Introduction to Partial Differential Equations. Princeton University Press, Princeton.
11. Friedman, A., Vogelius, M. (1989): Identification of small inhomogenities of extreme conductivity by boundary measurements: a theorem on continuous dependence. Arch. Ration. Mech. Anal. **105**, 299–326.
12. Gisser, D. G., Isaacson, D., Newell, J. C. (1990): Electric current computed tomography and eigenvalues. SIAM J. Appl. Math. **50**, 1623–1634.
13. Kato, T. (1966): Perturbation Theory for Linear Operators. Springer, Berlin.
14. Kirsch, A. (1998): Characterization of the shape of the scattering obstacle using the spectral data of the far field operator. Inverse Probl. **14**, 1489–1512.
15. Miranda, C. (1970): Partial Differential Equations of Elliptic Type. Springer, Berlin, 2nd ed.
16. Movchan, A. B., Serkov, S. K. (1997): The Pólya-Szegö matrices in asymptotic models of dilute composites. Eur. J. Appl. Math. **8**, 595–621.
17. Vogelius, M. S., Volkov, D. (2000): Asymptotic formulas for perturbations in the electromagnetic fields due to the presence of inhomogeneities of small diameter. RAIRO, Modélisation Math. Anal. Numér. **34**, 723–748.